Machine Learning Control Design for Elastic Composite Materials*

Sebastián Ossandón[1], Mauricio Barrientos[1], and Camilo Reyes[2]

[1] Instituto de Matemáticas, Pontificia Universidad Católica de Valparaíso, Blanco Viel 596, CerroBarón, Valparaíso, Chile
[2] Facultad de Ingeniería, Ciencia y Tecnología, Universidad Bernardo O'Higgins, Avenida Viel 1497, Santiago, Chile

Abstract. A novel numerical method, based on a machine learning approach, is used to solve an inverse problem involving the Dirichlet eigenfrequencies for the elasticity operator in a bounded domain filled with a composite material. The inhomogeneity of the material under study is characterized by a vector which is designed to control the constituent mixture of homogeneous elastic materials that compose it. Using the finite element method, we create a training set for a forward artificial neural network, solving the forward problem. A forward nonlinear map of the Dirichlet eigenfrequencies as a function of the vector design parameter is then obtained. This forward relationship is inverted and used to obtain a training set for an inverse radial basis neural network, solving the aforementioned inverse problem. A numerical example showing the applicability of this methodology is presented.

Keywords: Machine Learning · Composite Materials · Inverse Problems · Eigenfrequencies of the Elasticity Operator · Finite Element Method.

1 Introduction

Inverse problems applied to elasticity are usually promoted by the need to capture relevant information concerning the features and design parameters of the elastic materials under study. There has been a great body of research related to this problem, which the following ones can be mentioned:

- Reconstruction of inclusions (see [2] and [4])
- Non-destructive evaluation for mechanical structures (see [21])
- Parametric identification for elastic models: Lamé coefficients, elastic moduli, Poisson's ratio, mass density or wave velocity (see [3])
- Reconstruction of residual stresses (see [6])
- Model updating: dynamic control for mechanical structures ([9])

On the other hand, the use of spectral analysis to address elasticity problems is not new, for example, Babuška [5], Zienkiewicz ([37], [38]), Oden [24] and

* European Union's Horizon 2020 research and innovation programme under the Marie Sklodowska-Curie grant agreement No. 777778: MATHROCKS PROJECT.

ICCS Camera Ready Version 2021
To cite this paper please use the final published version:
DOI: 10.1007/978-3-030-77964-1_34

Boffi ([10], [12]), have analyzed the calculation of eigenfrequencies and eigenfunctions using this numerical technique. Also, see Sun and Zhou [31] and references therein. Forward numerical simulations of composites materials with local and well-defined inhomogeneities have been widely applied through the Finite Element Method (FEM), see for example Hassell and Sayas [20], Xu et al. [32] and Rodrigues et al. [29]. However applications of this method for composite (or inhomogeneous) materials is more complex. One of the reasons is that in anisotropic and composite (or inhomogeneous) materials, the models and the result interpretation are not easy to obtain using FEM, see Yan [33], Eigel and Peterseim [16], Choi [14] and Zhou et al. [36]. Consequently, FEM is not able to give an easy way to control the constituent mixture of composite materials.

Nowadays, machine learning algorithms (based on Artificial Neural Network (ANN)) are widely used in many problems. In Griffiths et al.[19] the solution of cornea curvature using a meshless method is discussed. In Liu et al. [22] a deep material network, is developed based on mechanistic homogenization theory of representative volume element and advanced machine learning techniques. The use of neural networks to solve the Stokes and Navier Stokes forward problems is studied in Baymani et al. ([7], [8]). The results show that the neural network has higher accuracy than classical methods. In Ossandón and Reyes [25], Ossandón et al. ([26] and [28]) the researchers solve the inverse eigenfrequency problems for the linear elasticity operator, the anisotropic Laplace operator, and the Stokes operator, respectively. Moreover, Ossandón et al. [27] solve an inverse problem to calculate the potential coefficients associated with the Hamiltonian operator in quantum mechanics.

In this article we are interested, in applying a machine learning approach, to obtain a vector of design parameters $\boldsymbol{\alpha} = (\alpha_1, \alpha_2, \cdots, \alpha_m)^{\mathbf{T}} \in \mathbb{R}^m$, which characterizes the thicknesses between the interfaces (we assume m interfaces) of each elastic homogeneous material that make up the composite material under study, as a function of eigenfrequencies of the elasticity operator. We note that $\boldsymbol{\alpha}$ is a vector of design parameters which control the constituent mixture of the composite material. The methodology proposed is based on the design of two ANNs (forward and inverse ANNs). The proposed ANNs are multilayered Radial-Basis Function (RBF) networks, and they are chosen due to the nature of the problem that is analyzed and the features exhibited by the neural network (see Schilling et al. [30] and Al-Ajlouni et al.[1]). Our main goal pursued with this article is to prove the effectiveness of the machine learning approach, evaluating its speed and accuracy in comparison with an approach based only on FEM. Therefore given a desired spectral behavior of the analyzed material, a specific composition for the mixture can be determined calculating $\boldsymbol{\alpha}$. The successful application of this methodology depends on the ability to face real inverse problem, specifically acquiring the eigenfrequencies associated with the elastic composite materials under study. In practice, using devices (or mechanisms) that use piezoelectric transducers, we can measure both the eigenfrequencies and the design parameters. Usually, the functioning of these mechanisms is based on resonance techniques such as resonant ultrasound spectroscopy (see [34] and [35]).

ICCS Camera Ready Version 2021
To cite this paper please use the final published version:
DOI: 10.1007/978-3-030-77964-1_34

The article is organized as follows: first we start with a machine learning analysis to solve general inverse problems which is described in section 2. The constitutive relations for elastic composite materials are described in section 3, on the other hand in section 4 we introduce the corresponding forward and inverse problems, and its respective solutions are displayed in sections 5 and 6. In section 7, a numerical example is exposed, and finally the conclusions follow in section 8. Figure 1 shows an example of the type of composite material this article is analyzing, which is composed by homogenous domains.

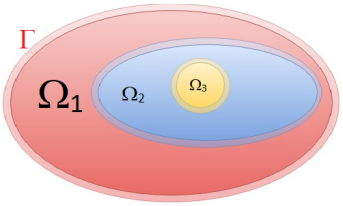

Fig. 1. Elastic composite material.

2 Solving inverse problems using machine learning algorithms

Mathematically, solving an inverse problem consists of estimating a signal P from data observations M where:

$$\mathcal{F}_T(\mathrm{P}) = \mathrm{M}, \qquad \mathrm{P} \in \mathbb{X} \quad \text{and} \quad \mathrm{M} \in \mathbb{Y}. \tag{1}$$

In equation (1), $\mathbb{X}$ and $\mathbb{Y}$ are vector spaces with norm, and $\mathcal{F}_T : \mathbb{X} \to \mathbb{Y}$ is called the forward operator. Let us observe that the forward operator has been parametrized by T. For example in some non-destructive evaluation problems, T denotes a well-known trajectory composed of several transmitter and receiver locations (sensor locations).

Machine learning methodology can be used in order to obtain (approximately) a non-linear mapping $\mathcal{F}^{\dagger}_{T,\theta} : \mathbb{Y} \to \mathbb{X}$ satisfying:

$$\mathcal{F}^{\dagger}_{T,\theta}(\mathrm{M}) \approx \mathrm{P}_{\mathrm{seek}}, \qquad \mathrm{M} \in \mathbb{Y} \quad \text{and} \quad \mathrm{P}_{\mathrm{seek}} \in \mathbb{X}. \tag{2}$$

Let us observe that $\mathcal{F}^{\dagger}_{T,\theta}$ (which is an ANN) has been parametrized also by T and by $\theta \in \Theta$. The main idea when we use machine learning algorithms is to make a choice of an optimal parameter $\theta^* \in \Theta$ given some training data. This optimal parameter can be obtained by minimizing a functional to control the quality of a learned $\mathcal{F}^{\dagger}_{T,\theta}$. In other words, we propose solving the inverse problem using machine learning algorithms amounts to learn $\mathcal{F}^{\dagger}_{T,\theta}$ from data such that it approximates an inverse of $\mathcal{F}_T$.

ICCS Camera Ready Version 2021
To cite this paper please use the final published version:
DOI: 10.1007/978-3-030-77964-1_34

We assume that the metric spaces $\mathbb{X}$ and $\mathbb{Y}$ are endowed with the respective norms: $\|\cdot\|_{\mathbb{X}} : \mathbb{X} \to \mathbb{R}$ and $\|\cdot\|_{\mathbb{Y}} : \mathbb{Y} \to \mathbb{R}$.

2.1 Supervised learning

In supervised learning the input/output data set are known. The optimization (minimization) problem that we propose to solve is:

$$\min_{\theta\in\Theta}\left\{\frac{1}{2}\|\mathcal{F}_T\circ\mathcal{F}^{\dagger}_{T,\theta}\circ\mathcal{F}_T(\mathrm{P})-\mathrm{M}\|^2_{\mathbb{Y}}+\beta\mathcal{R}_T(\mathrm{P})\right\}. \tag{3}$$

where the functional $\mathcal{R}_T : \mathbb{X} \to \mathbb{R}$ is known as a regularization functional that penalizes unfeasible solutions. The parameter β measures this penalization.

2.2 Unsupervised learning

In the case of unsupervised learning the output data set is unknown. For his problem we propose to minimize:

$$\min_{\theta\in\Theta}\left\{\frac{1}{2}\|\mathcal{F}_T\circ\mathcal{F}^{\dagger}_{T,\theta}\circ\mathcal{F}_T(\mathrm{P})-\mathcal{F}_T(\mathrm{P})\|^2_{\mathbb{Y}}+\beta\mathcal{R}_T(\mathrm{P})\right\}, \tag{4}$$

Let us notice that in many cases it can be quite complicated to use directly $\mathcal{F}_T$ in the optimization algorithm, which can be a minimizing numerical method. In these cases, it is convenient to also use an approximation (another ANN) $\mathcal{F}_{T,\theta_1}$ for $\mathcal{F}_T$. In addition, if this new network (called forward ANN) is well trained, we can greatly reduce the calculation time involved in solving many times many forward problems.

Finally, we must indicate that since in general the forward problems are well-posed, the use of the operator $\mathcal{F}_T \circ \mathcal{F}^{\dagger}_{T,\theta} \circ \mathcal{F}_T$ in the optimization problem limits the existence of unfeasible solutions, which together with the use of an additional regularization functional $\mathcal{R}_T$ could be suitable for choosing a "good physical" solution for the inverse problem.

3 Constitutive relations in elasticity

Let $\Omega \subset \mathbb{R}^l$ ($l = 2$ or 3) be a nonempty, open, convex and bounded domain, with its regular boundary Γ, filled with an elastic composite material characterized by its Lamé functions $\gamma_{\boldsymbol{\alpha}}(\boldsymbol{x})$, $\mu_{\boldsymbol{\alpha}}(\boldsymbol{x})$ ($\boldsymbol{x} \in \Omega$). In this work, $\boldsymbol{\alpha}$ is a designed vector of parameters used to modify the spectral response (eigenfrequencies and eigenfunctions) associated to an elastic material through the control of its constituent mixture.

We denote the elastic composite tensor, for an isotropic medium, by $\boldsymbol{C}^{\boldsymbol{\alpha}}_{ijrq}(\boldsymbol{x}) = \gamma_{\boldsymbol{\alpha}}(\boldsymbol{x})\delta_{ij}\delta_{rq} + \mu_{\boldsymbol{\alpha}}(\boldsymbol{x})(\delta_{jr}\delta_{iq} + \delta_{iq}\delta_{ir})$ ($1 \leqslant i, j, r, q \leqslant l$), where $\delta_{\cdot,\cdot}$ is the Kronecker delta function. We remark that this tensor is positive definite.

ICCS Camera Ready Version 2021
To cite this paper please use the final published version:
DOI: 10.1007/978-3-030-77964-1_34

The generalized Hooke's law, relating the mechanical displacements $\boldsymbol{u}$ ($\boldsymbol{u}(\boldsymbol{x})$) with the associated stress tensor $\boldsymbol{\sigma}^{\boldsymbol{\alpha}}$ ($\boldsymbol{\sigma}^{\boldsymbol{\alpha}}(\boldsymbol{x},\boldsymbol{u}) = \gamma_{\boldsymbol{\alpha}}(\boldsymbol{x})(\nabla\cdot\boldsymbol{u})\mathcal{I} + 2\mu_{\boldsymbol{\alpha}}(\boldsymbol{x})\mathcal{E}(\boldsymbol{u})$) is given by:

$$\boldsymbol{\sigma}^{\boldsymbol{\alpha}}_{ij}(\boldsymbol{x},\boldsymbol{u}) = \boldsymbol{\sigma}^{\boldsymbol{\alpha}}_{ji}(\boldsymbol{x},\boldsymbol{u}) = \sum_{r,q} \boldsymbol{C}^{\boldsymbol{\alpha}}_{ijrq}(\boldsymbol{x})\mathcal{E}_{rq}(\boldsymbol{u}), \tag{5}$$

where:

$$\mathcal{E}_{ij}(\boldsymbol{u}) = \frac{1}{2}\left(\partial_j u_i + \partial_i u_j\right) \tag{6}$$

is the strain tensor.

4 The forward and inverse problems

4.1 The forward problem

As a forward problem, we consider the following eigenfrequency problem: given $\boldsymbol{\alpha} \in \mathbb{R}^m_+$, find $\lambda \in \mathbb{R}$ and the non-null valued functions $\boldsymbol{u}$ which are the solutions of:

$$\begin{cases} -\mathrm{div}(\gamma_{\boldsymbol{\alpha}}(\boldsymbol{x})(\nabla\cdot\boldsymbol{u})\mathcal{I} + 2\mu_{\boldsymbol{\alpha}}(\boldsymbol{x})\mathcal{E}(\boldsymbol{u})) = \lambda\boldsymbol{u} & \text{for} \quad \boldsymbol{x} \in \Omega\,, \\ \qquad\qquad\qquad\qquad\qquad\quad \boldsymbol{u} = \boldsymbol{0} & \text{for} \quad \boldsymbol{x} \in \Gamma\,. \end{cases} \tag{7}$$

where $\mathcal{I}$ is the identity matrix of size $l \times l$.

We note (see [5]) that the only non-null solutions of (7) are a countable pair sequence $\{(\lambda_n, \boldsymbol{u}_n\}_{n\geqslant 1}$ of eigenfrequencies and eigenfunctions.

We define the function $\mathcal{F}_N$ associated with (7):

$$\mathcal{F}_N : \mathbb{R}^m_+ \to \mathbb{R}^N, \quad \overrightarrow{\boldsymbol{\lambda}}^N := (\lambda_1, \lambda_2, \cdots, \lambda_N)^{\mathbf{T}} = \mathcal{F}_N(\boldsymbol{\alpha}). \tag{8}$$

We remark that the function $\mathcal{F}_N$ ($N \in \mathbb{N}$) solves the forward problem associated to (7).

4.2 The inverse problem

We consider the following inverse problem associated to (7):

Find $\boldsymbol{\alpha} \in \mathbb{R}^m_+$ such that

$$\begin{cases} -\mathrm{div}(\gamma_{\boldsymbol{\alpha}}(\boldsymbol{x})(\nabla\cdot\boldsymbol{u}^d_n)\mathcal{I} + 2\mu_{\boldsymbol{\alpha}}(\boldsymbol{x})\mathcal{E}(\boldsymbol{u}^d_n)) = \lambda^d_n\,\boldsymbol{u}^d_n & \text{in} \quad \Omega, \\ \qquad\qquad\qquad\qquad\quad \boldsymbol{u}^d_n = \boldsymbol{0} & \text{on} \quad \Gamma, \end{cases} \tag{9}$$

where the given pair $\left\{\lambda^d_n, \boldsymbol{u}^d_n\right\}_n$, with $n \in \mathbb{N}$ and $n \leq N < +\infty$, characterizing the desired spectral behavior.

We define the function $\mathcal{F}_N^{-1}$, which is the inverse function of $\mathcal{F}_N$, associated to (9):

ICCS Camera Ready Version 2021
To cite this paper please use the final published version:
DOI: 10.1007/978-3-030-77964-1_34

$$\mathcal{F}_N^{-1} : \mathbb{R}^N \to \mathbb{R}_+^m, \quad \boldsymbol{\alpha} = \mathcal{F}_N^{-1}(\overrightarrow{\boldsymbol{\lambda}}^N). \tag{10}$$

We remark that the function $\mathcal{F}_N^{-1}$ ($N \in \mathbb{N}$) solves the inverse problem associated to (9).

5 Solution of the forward problem

5.1 Variational Formulation

We define the functional space

$$\mathbf{V} = \mathbf{U} = \left\{ \boldsymbol{v} = (v_1, v_2, \cdots, v_l) \in [H^1(\Omega)]^l; \quad v_i = 0 \quad \text{on} \quad \Gamma, \quad 1 \leqslant i \leqslant l \right\}, \tag{11}$$

associated with the norm $\|\boldsymbol{v}\|_{1,\Omega}^2 = (\sum_{i=1}^{l} \|v_i\|_{1,\Omega}^2)^{1/2}$.

The corresponding variational form of equation (7) is given by:

$$a_{\boldsymbol{\alpha}}(\boldsymbol{u}, \boldsymbol{v}) := \int_\Omega (\gamma_{\boldsymbol{\alpha}}(\boldsymbol{x})(\nabla \cdot \boldsymbol{u})(\nabla \cdot \boldsymbol{v}) + 2\mu_{\boldsymbol{\alpha}}(\boldsymbol{x})\mathcal{E}(\boldsymbol{u}) : \mathcal{E}(\boldsymbol{v}))dx = \lambda \int_\Omega \boldsymbol{u} \cdot \boldsymbol{v} dx. \tag{12}$$

Thus the weak formulation for the eigenfrequency problem in elasticity, considering homogeneous boundary conditions, is given by: *Find* $(\lambda, \boldsymbol{u}) \in (\mathbb{R}, \mathbf{U})$ *such that*

$$a_{\boldsymbol{\alpha}}(\boldsymbol{u}, \boldsymbol{v}) = \lambda\, (\boldsymbol{u}, \boldsymbol{v})_{0,\Omega} \qquad \forall \boldsymbol{v} \in \mathbf{V}, \tag{13}$$

where $(\cdot, \cdot)_{0,\Omega}$ is the inner product of $[L^2(\Omega)]^l$.

5.2 Discretization

To obtain the discrete form of the variational formulation (13), the approach is based on $\mathbb{P}_k$-Lagrange Finite Element ($k \geqslant 1$) in Ω is used.

Let $\{\mathcal{T}_h\}_{h>0}$ be a regular mesh discretizing Ω (see Ciarlet [15]), composed by triangles T_i ($i = 1, ..., M_h$) of diameter h_{T_i}, such that $h := \sup_{T_i \in \mathcal{T}_h} h_{T_i}$ measures the size of the mesh $\mathcal{T}_h$. Furthermore, we consider the finite element space $\mathbf{V}_h \subset \mathbf{V}$ of piecewise polynomials $\mathbb{P}_k$ ($k \geqslant 1$).

Let $(\lambda_h, \boldsymbol{u}_h) \in (\mathbb{R}, \mathbf{V}_h)$ be the eigenpair solution to the discrete weak form of (13). The Rayleigh quotient for each discrete eigenfrequency λ_h is given by:

$$\lambda_h = \frac{a_{\boldsymbol{\alpha}}(\boldsymbol{u}_h, \boldsymbol{u}_h)}{(\boldsymbol{u}_h, \boldsymbol{u}_h)_{0,\Omega}} = \mathcal{F}_N(\boldsymbol{\alpha})\ . \tag{14}$$

Finally, let us mention that the Babuska-Brezzi condition (see [5], [10], [11], [13], [15] and [23]) satisfied by the approximation spaces, ensures the wellposedness of the discrete weak form of (13).

ICCS Camera Ready Version 2021
To cite this paper please use the final published version:
DOI: 10.1007/978-3-030-77964-1_34

6 Solution of the inverse problem using machine learning

A the machine learning approach can be used to solve the inverse problem previously discussed. Afterwards a the machine learning algorithm can reconstruct the nonlinear inverse mapping $\mathcal{F}^{\dagger}_{\boldsymbol{\theta},N} : \mathbb{R}^N \to \mathbb{R}^m_+$ that approximate $\mathcal{F}_N^{-1}$ above defined. Let $\mathcal{F}^{\dagger}_{\boldsymbol{\theta},N}$ be an inverse Artificial Neural Network (ANN) with activation functions defined by a Radial Based Function (RBF). The structure will consist in one input layer containing n neurons, one hidden layer containing s neurons and an output layer containing m neurons. Let us notice that $\boldsymbol{\theta}$ is a vector parameter associated with the specific network topology. The use of this type of ANN is treated by Girosi et al. [17] and Girosi and Poggio [18]. In these articles, the authors analyze, in detail, the regularization features of an RBF ANN.

To perform the construction of the above inverse network (which solves the inverse problem), we define a forward RBF ANN $\mathcal{F}_{\boldsymbol{\theta}_1,N} : \mathbb{R}^m_+ \to \mathbb{R}^N$, used as an approximation of the direct operator $\mathcal{F}_N$, with one hidden layer containing s_1 neurons and one output layer containing N neurons. Let us remark that, we use the forward network $\mathcal{F}_{\boldsymbol{\theta}_1,N}$ instead of $\mathcal{F}_N$ to accelerate the calculation of eigenfrequencies. In this case $\boldsymbol{\theta}_1$ is a vector parameter associated to the topology of $\mathcal{F}_{\boldsymbol{\theta}_1,N}$. An optimal estimation for $\boldsymbol{\theta}_1$ is given by:

$$\boldsymbol{\theta}_1^* = \min_{\boldsymbol{\theta}_1} \left\{ \frac{1}{2} \|\mathcal{F}_N(\boldsymbol{\alpha}) - \mathcal{F}_{\boldsymbol{\theta}_1,N}(\boldsymbol{\alpha})\|^2_{\mathbb{R}^N} \right\}. \tag{15}$$

Once calculated $\boldsymbol{\theta}_1^*$, we can obtain an optimal estimation for $\boldsymbol{\theta}$ using:

$$\boldsymbol{\theta}^* = \min_{\boldsymbol{\theta}} J(\boldsymbol{\theta}) = \min_{\boldsymbol{\theta}} \left\{ \frac{1}{2} \|\mathcal{F}_{\boldsymbol{\theta}_1^*,N}(\boldsymbol{\alpha}) - \mathcal{F}_{\boldsymbol{\theta}_1^*,N} \circ \mathcal{F}^{\dagger}_{\boldsymbol{\theta},N} \circ \mathcal{F}_{\boldsymbol{\theta}_1^*,N}(\boldsymbol{\alpha})\|^2_{\mathbb{R}^N} \right\}. \tag{16}$$

Obtaining $\boldsymbol{\theta}_1^*$ and $\boldsymbol{\theta}^*$ is usually known as the training process associated with the forward and inverse networks respectively. Let us notice that the training process can be performed, for example, using a backpropagation algorithm (see [17] and [18]): starting with an initial parameter vector $\boldsymbol{\theta}^0$, the training algorithm iteratively decreases the mean square error updating $\boldsymbol{\theta}$, where each iteration is given as follows:

$$\boldsymbol{\theta}^{i+1} = \boldsymbol{\theta}^i - \epsilon \mathbf{L} \cdot \frac{\partial J(\boldsymbol{\theta}^i)}{\partial \boldsymbol{\theta}^i}, \tag{17}$$

where ϵ controls the length of the update increment and $\mathbf{L}$ is a matrix that defines the backpropagation algorithm to be used.

Finally, we remark that the regularization functional $\mathcal{R}_T$ for our specific problem is not required because $\mathcal{F}_{\boldsymbol{\theta}_1^*,N} \circ \mathcal{F}^{\dagger}_{\boldsymbol{\theta}^*,N} \circ \mathcal{F}_{\boldsymbol{\theta}_1^*,N}$ (from its definition) only allows the "good physical" solution.

ICCS Camera Ready Version 2021
To cite this paper please use the final published version:
DOI: 10.1007/978-3-030-77964-1_34

7 Numerical result

Let us consider the problem (7), where $\Omega =]1,3[\times]1,2[\subset \mathbb{R}^2$ ($\boldsymbol{x} = (x,y)^\top$) and $\Gamma = \overline{\Omega} - \Omega$. A representative diagram showing the domain of our example is the Figure 2. Figure 3 shows the function that models the interfaces between each of the homogenous domains. In this example $\boldsymbol{\alpha} = (\alpha_1, \alpha_2)^{\mathbf{T}} = (\alpha, \alpha)^{\mathbf{T}}$.

Let us assume that $\gamma_j = \frac{\nu_j E_j}{(1+\nu_j)(1-2\nu_j)}, \mu_j = \frac{E_j}{2(1+\nu_j)}$ $(1 \leqslant j \leqslant 3)$, where E_j is the Young's modulus and ν_j is the Poisson's ratio for the elastic homogeneous material of the domain Ω_j (see Figure 2). Table 1 shows the values for E_j and ν_j $(1 \leqslant j \leqslant 3)$ used in our example.

Table 1. Coefficients used in this numerical example.

Material	**E (Young's modulus)** GPa	ν **(Poisson's ratio)**
Cooper ($j = 1$)	124	0.34
Stainless steel ($j = 2$)	200	0.30
Aluminum ($j = 3$)	79	0.35

Let us define:

$$\tilde{\Omega}_{\alpha,1}(\boldsymbol{x}) = \begin{cases} 1 & \text{if} \quad 1 < x \leqslant 1.5 - \dfrac{\alpha}{2}, 1 < y < 2.0, \\ \dfrac{1.5 + \frac{\alpha}{2} - x}{\alpha} & \text{if} \quad 1.5 - \dfrac{\alpha}{2} < x \leqslant 1.5 + \dfrac{\alpha}{2}, 1 < y < 2.0, \\ 0 & \text{if} \quad 1.5 + \dfrac{\alpha}{2} < x < 3.0, 1 < y < 2.0, \end{cases} \tag{18}$$

$$\tilde{\Omega}_{\alpha,2}(\boldsymbol{x}) = \begin{cases} 0 & \text{if} \quad 1 < x \leqslant 1.5 - \dfrac{\alpha}{2}, 1 < y < 2.0, \\ \dfrac{x - 1.5 + \frac{\alpha}{2}}{\alpha} & \text{if} \quad 1.5 - \dfrac{\alpha}{2} < x \leqslant 1.5 + \dfrac{\alpha}{2}, 1 < y < 2.0, \\ 1 & \text{if} \quad 1.5 + \dfrac{\alpha}{2} < x \leqslant 2.5 - \dfrac{\alpha}{2}, 1 < y < 2.0, \\ \dfrac{2.5 + \frac{\alpha}{2} - x}{\alpha} & \text{if} \quad 2.5 - \dfrac{\alpha}{2} < x \leqslant 2.5 + \dfrac{\alpha}{2}, 1 < y < 2.0, \\ 0 & \text{if} \quad 2.5 + \dfrac{\alpha}{2} < x < 3.0, 1 < y < 2.0, \end{cases} \tag{19}$$

and

$$\tilde{\Omega}_{\alpha,3}(\boldsymbol{x}) = \begin{cases} 0 & \text{if} \quad 1 < x \leqslant 2.5 - \dfrac{\alpha}{2}, 1 < y < 2.0, \\ \dfrac{x - 2.5 + \frac{\alpha}{2}}{\alpha} & \text{if} \quad 2.5 - \dfrac{\alpha}{2} < x \leqslant 2.5 + \dfrac{\alpha}{2}, 1 < y < 2.0, \\ 1 & \text{if} \quad 2.5 + \dfrac{\alpha}{2} < x < 3.0, 1 < y < 2.0. \end{cases} \tag{20}$$

ICCS Camera Ready Version 2021
To cite this paper please use the final published version:
DOI: 10.1007/978-3-030-77964-1_34

Note that $\sum_{j=1}^{3} \tilde{\Omega}_{\alpha,j}(\boldsymbol{x}) = 1$.

The relationships $\tilde{\Omega}_{\alpha,j}(x), 1 \leqslant j \leqslant 3$ are functions related to sets $\Omega_j, 1 \leqslant j \leqslant 3$ (see Figure 3) where a1 $= 1.5 - \frac{\alpha}{2}$, a2 $= 1.5 + \frac{\alpha}{2}$, a3 $= 2.5 - \frac{\alpha}{2}$ and a4 $= 2.5 + \frac{\alpha}{2}$ respectively. These functions (which are a partition of the unity) are employed with the purpose to model the constituent mixture of homogeneous materials in order to obtain composite materials with new physical properties. It is important to remark that inhomogeneities considered in this example only depend only on the x variable and do not depend on y variable (see Figure 2).

We also define the variable Lamé coefficients characterizing the inhomogeneities of elastic materials understudy

$$\gamma_\alpha(\boldsymbol{x}) = \frac{\sum_{j=1}^{3} \gamma_j \tilde{\Omega}_{\alpha,j}(\boldsymbol{x})}{\sum_{j=1}^{3} \tilde{\Omega}_{\alpha,j}(\boldsymbol{x})} \quad \text{and} \quad \mu_\alpha(\boldsymbol{x}) = \frac{\sum_{j=1}^{3} \mu_j \tilde{\Omega}_{\alpha,j}(\boldsymbol{x})}{\sum_{j=1}^{3} \tilde{\Omega}_{\alpha,j}(\boldsymbol{x})}, \tag{21}$$

In this example, the thickness α = a2-a1 = a4-a3 is the design parameter used to control the constituent mixture of the composite material. Let us observe that:

$$\lim_{\alpha \to 0} \gamma_\alpha(\boldsymbol{x}) = \sum_{j=1}^{3} \gamma_j \mathbf{1}_{\Omega_j}(\boldsymbol{x}) \quad \text{and} \quad \lim_{\alpha \to 0} \mu_\alpha(\boldsymbol{x}) = \sum_{j=1}^{3} \mu_j \mathbf{1}_{\Omega_j}(\boldsymbol{x}) \tag{22}$$

where

$$\mathbf{1}_{\Omega_1}(\boldsymbol{x}) = \begin{cases} 1 & \text{if} \quad 1 < x < 1.5, y \in]1,2[, \\ 0.5 & \text{if} \quad x = 1.5, y \in]1,2[, \\ 0 & \text{elsewhere}, \end{cases} \tag{23}$$

$$\mathbf{1}_{\Omega_2}(\boldsymbol{x}) = \begin{cases} 1 & \text{if} \quad 1.5 < x < 2.5, y \in]1,2[, \\ 0.5 & \text{if} \quad x = 1.5, y \in]1,2[, \\ 0.5 & \text{if} \quad x = 2.5, y \in]1,2[, \\ 0 & \text{elsewhere}, \end{cases} \tag{24}$$

and

$$\mathbf{1}_{\Omega_3}(\boldsymbol{x}) = \begin{cases} 1 & \text{if} \quad 2.5 < x < 3.0, y \in]1,2[, \\ 0.5 & \text{if} \quad x = 2.5, y \in]1,2[, \\ 0 & \text{elsewhere}. \end{cases} \tag{25}$$

The purpose of this example is to obtain numerically a specific composition for the mixture (calculating α) with a desired spectral behavior of the composite material (solve the inverse problem).

The forward RBF ANN $\mathcal{F}_{\boldsymbol{\theta}_1,N}$ is trained with data provided by simulations obtained using FEM ($\mathbb{P}_2$ finite elements): $\alpha^{(i)} = 0.4 - 0.02(i-1)$, $(\overrightarrow{\boldsymbol{\lambda}}^N)^{(i)} = \mathcal{F}_N(\alpha^{(i)}), 1 \leqslant i \leqslant N_1$, being in this case $N_1 = 20$. We use equation (15), applying the backpropagation algorithm for the training data, in order to obtain the optimal vector parameter $\boldsymbol{\theta}_1^*$ (associated with the forward RBF ANN topology) and

ICCS Camera Ready Version 2021
To cite this paper please use the final published version:
DOI: 10.1007/978-3-030-77964-1_34

performing the approximation for $\mathcal{F}_N$. After training the forward network, we use it to simulate a larger amount of data $N_2 >> N_1$, with $\alpha^{(i)} = 0.4 - 0.002(i-1)$ $(1 \leqslant i \leqslant N_2 = 200)$, to obtain a set of training data for the construction of the inverse RBF ANN $\mathcal{F}^{\dagger}_{\boldsymbol{\theta},N}$. In this case we also use the backpropagation algorithm in the training process, using equation (16) to obtain the optimal vector parameter $\boldsymbol{\theta}^*$ (associated with the inverse RBF ANN topology). Finally, we have the inverse network trained and we can use it to solve numerically the inverse problem. Figure 4 shows a comparison of the evolution, when the value of the simulated data is $N_s = 2000$ and $\alpha^{(i)} = 0.4 - 0.0002(i-1)$, $1 \leqslant i \leqslant N_s$, of the first 4 Dirichlet eigenfrequencies: 1) directly calculated using the FEM and 2) calculated from the forward RBF ANN with the data input obtained from the ANN: $\mathcal{F}_{\boldsymbol{\theta}^*_1,N} \circ \mathcal{F}^{\dagger}_{\boldsymbol{\theta}^*,N} \circ \mathcal{F}_{\boldsymbol{\theta}^*_1,N}(\alpha^{(i)})$. As seen in this figure, the Dirichlet eigenfrequencies calculated using ANNs approximate quite well the calculated Dirichlet eigenfrequencies using FEM. However when $\alpha \to 0$ the accuracy of the approximation decreases. This problem can be solved increasing the size of the data set as α converges to zero.

The computational performance is summarized in table 2. The merit figure used are the mean squared error (MSE) and the computational time (using ANN: CT ANN) vs FEM: CT FEM), required for the simulations of our example. Let us notice that CT ANN is calculated taking into account the computational time required to obtain the training data set, using the FEM results, which are needed by the forward RBF ANN. Let us observe the CT ANN compared with the CT FEM (CT ANN << CT FEM), remarking the good computational performance attained using the MSE. It is important to remark that the difference between the data set prepared using FEM ($N_1 = 20$) and the data set used for the simulation ($N_s = 2000$) in this example, implies the difference between the computational times CT ANN and CT FEM, and also the MSE. It is possible to improve the MSE by increasing N_1, implying a longer training time for the forward RBF ANN, and thus increasing the CT ANN.

The computer, used to obtain the results shown in this section, has a 2.4 GHz Intel Core Duo processors with 3GB of RAM.

Table 2. Computational performance summary.

N_s	MSE: $\frac{1}{N_s}\sum_{i=1}^{N_s}(\alpha^{(i)} - \widehat{\alpha}^{(i)})^2$	CT ANN (seconds)	CT FEM (seconds)
2000	$1.8440e-06$	65.9468	5330.69

8 Conclusion

A novel numerical method, based on a machine learning approach, is used to solve an inverse problem associated with the calculation of the Dirichlet eigenfrequencies for the elasticity operator in a bounded domain filled with a composite

ICCS Camera Ready Version 2021
To cite this paper please use the final published version:
DOI: 10.1007/978-3-030-77964-1_34

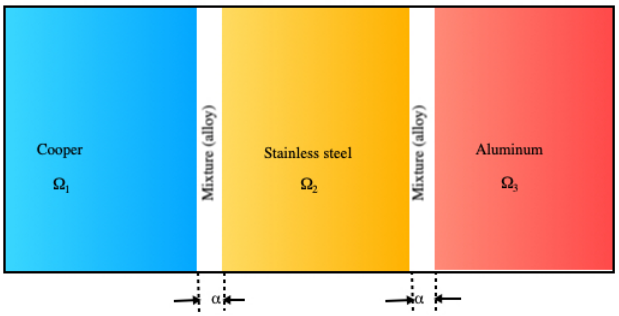

Fig. 2. Composite material used in the numerical example.

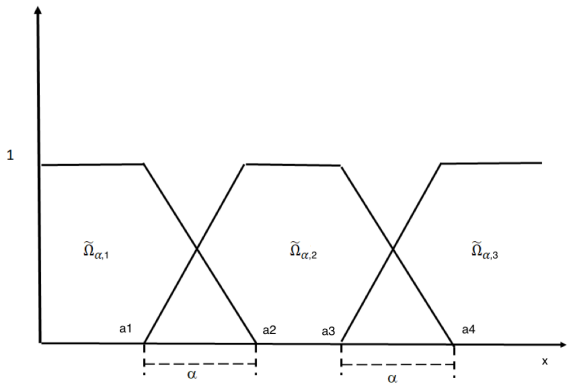

Fig. 3. Functions used in the numerical example.

material. The numerical results shows that the calculation, using RBF ANNs, of the vector of design parameters $\boldsymbol{\alpha} = (\alpha_1, \alpha_2)^{\mathbf{T}} = (\alpha, \alpha)^{\mathbf{T}}$ (in this case α is the thickness between the interfaces of each homogeneous material that compose the material used in the numerical example) from the eigenfrequencies of the elastic composite material, has a relatively negligible error and clearly the time consumption performance shows very important improvements compared to a more traditional approach based only on FEM (see Table 2). In summary, we have proved the effectiveness of a method that can be used as a control design tool: given a desired spectral response, we can control (motivated for the design) the constituent mixture of an elastic composite material. The method improves time performance without compromising the accuracy of the numerical results.

ICCS Camera Ready Version 2021
To cite this paper please use the final published version:
DOI: 10.1007/978-3-030-77964-1_34

Finally, as a consequence of the notable improvements in the time calculation of our methodology, it can be used, in future works, to design real-time controllers for the mixture of composite materials.

Acknowledgements

S. Ossandón acknowledges support from the European Union's Horizon 2020 research and innovation programme under the Marie Sklodowska-Curie grant agreement No. 777778: MATHROCKS PROJECT.

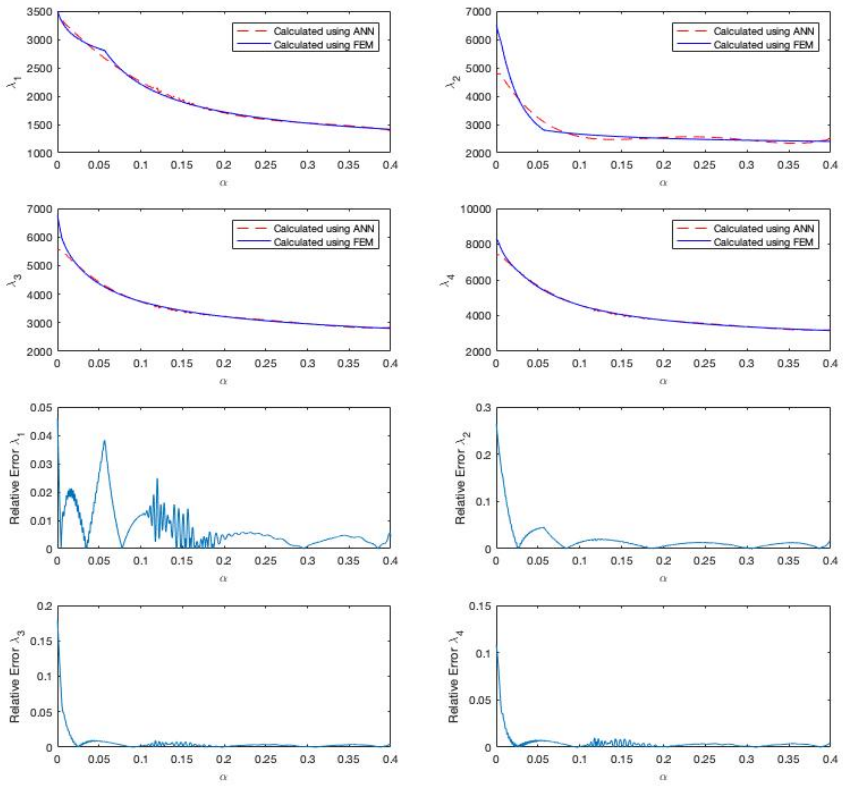

Fig. 4. Comparison of the first 4 calculated eigenfrequencies.

References

1. Al-Ajlouni, A.-F., Schilling, R.- J., Harris, S.-L.: Identification of nonlinear discrete-time systems using raised-cosine radial basis function networks. International Jour-

ICCS Camera Ready Version 2021
To cite this paper please use the final published version:
DOI: 10.1007/978-3-030-77964-1_34

nal of Systems Science **35**(4) 211-221 (2004).
2. Alves, C.- J. S., Antunes, P.-R. S.: The Method of Fundamental Solutions applied to the Calculation of Eigenfrequencies and eigenmodes of $2D$ simply connected shapes. CMC-Comp. Mat. & Contin. **2**(4) 251-265 (2005).
3. Ammari, H., Kang, H., Nakamura, G., Tanuma, K: Complete asymptotic expansions of solutions of the system of elastostatics in the presence of an inclusion of small diameter and detection of an inclusion. J. Elast. **67** 97-129 (2002).
4. Andrieux, S., Ben Abda, A., Bui, H.- D.: Sur l'identification de fissures planes via le concept d'écart à la réciprocité en élasticité, C.R. Acad. Sci. Paris, Série II **324** 1431-1438 (1997).
5. Babuška, I., Osborn, J.- E.: Eigenvalue Problems, Handbook of Numerical Analysis: Finite Element Methods (Part 1). Vol. 2, P. G. Ciarlet and J. L. Lions, eds., North-Holland, Amsterdam (2000).
6. Ballard, P., Constantinescu, A.: On the inversion of subsurface residual stresses from surface stress measurements. J. Mech. Phys. Solids **42** 1767-1788 (1994).
7. Baymani, M., Effati, S., Kerayechian, A.: A feed-forward neural network for solving Stokes problem. Acta Appl. Math. **116**(1) 55-64 (2011).
8. Baymani, M., Effati, S., Niazmand, H., Kerayechian, A.: Artificial neural network method for solving the Navier-Stokes equations. Neural Comput. Appl. **26** 765-773 (2015).
9. Ben Abdallah, J.: Inversion gaussienne appliquée à la correction paramétrique de modèles structuraux. Ph.D. thesis, Ecole Polytechnique, Paris, France (1995).
10. Boffi, D.: Finite element approximation of eigenvalue problems. Acta Numerica **19** 1-120 (2010).
11. Boffi, D., Brezzi, F., Fortin, M.: Mixed finite element methods and applications. Springer Series in Computational Mathematics, 44. Springer, Heidelberg (2013).
12. Boffi, D., Gastaldi, L.: Some remarks on finite element approximation of multiple eigenvalues. Appl. Numer. Math. **79** 18-28 (2014).
13. Brezzi, F., Fortin, M.: Mixed and Hybrid Finite Elements Methods, Springer-Verlag, Berlin (1991).
14. Choi, H.- J.: A numerical solution for the inhomogeneous Dirichlet boundary value problem on a nonconvex polygon. Applied Mathematics and Computation **341** 31-45 (2019).
15. Ciarlet, P.- G.: The Finite Element Method for Elliptic Problems. North-Holland, Amsterdam (1978).
16. Eigel, M., Peterseim, D.: Simulation of Composite Materials by a Nertwork FEM with Error Control. Computational Methods in Applied Mathematics **15**(1) 21-37 (2014).
17. Girosi, F., Jones, M., Poggio, T.: Regularization Theory and Neural Networks Architectures. J. Neural Computation **7** 219-269 (1995).
18. Girosi, F., Poggio, T.: A Theory of Networks for Approximation and Learning, MIT Artificial Intelligence Laboratory, A.I. Memo No.1140, C.B.I.P Paper No.31 (1989).
19. Griffiths, G.- W., Plociniczak, L., Schiesser, W.- E.: Analysis of cornea curvature using radial basis functions - Part I: Methodology. Computers in Biology and Medicine **77** 274-284 (2016).
20. Hassell, M.- E., Sayas, F.- J.: A fully discrete BEM-FEM scheme for transient acoustic waves. Computer Methods in Applied Mechanics and Engineering **309** 106-130 (2016).
21. Leonard, K.- R., Malyarenko, E.- V., Hinders, M.- K.: Ultrasonic Lamb wave tomography. Inverse Problems **18** 1795-1808 (2002).

ICCS Camera Ready Version 2021
To cite this paper please use the final published version:
DOI: 10.1007/978-3-030-77964-1_34

22. Liu, Z., Wu, C.- T., Koishi, M.: A deep material network for multiscale topology learning and accelerated nonlinear modeling of heterogeneous materials. Computer Methods in Applied Mechanics and Engineering, In Press https://doi.org/10.1016/j.cma.2018.09.020.
23. Mercier, B., Osborn, J., Rappaz, J., Raviart, P.- A.: Eigenvalue approximation by mixed and hybrid methods. Math. Comp. **36** 427-453 (1981).
24. Oden, J.- T., Reddy, J.- N.: An Introduction to the Mathematical Theory of Finite Elements, Wiley Interscience, New York (1976).
25. Ossandón, S., Reyes, C.: On the neural network calculation of the Lamé coefficients through eigenvalues of the elasticity operator. C. R. Mecanique **344** 113-118 (2016).
26. Ossandón, S., Reyes, C., Reyes, C.- M.: Neural network solution for an inverse problem associated with the Dirichlet eigenvalues of the anisotropic Laplace operator. Comput. Math. Appl. **72** 1153-1163 (2016).
27. Ossandón, S., Reyes, C., Cumsille, P., Reyes, C.- M.: Neural network approach for the calculation of potential coefficients in quantum mechanics. Comput. Phys. Commun. **214** 31-38 (2017).
28. Ossandón, S., Barrientos, M., Reyes, C.: Neural network solution to an inverse problem associated with the eigenvalues of the Stokes operator. C. R. Mecanique **346** 39-47 (2018).
29. Rodrigues, D.-E. S., Belinha, J., Pires, F.- M. A., Dinis, L.- M. J. S., Natal Jorge, R.- M.: Homogenization technique for heterogeneous composite materials using meshless methods. Engineering Analysis with Boundary Elements **92** 73-89 (2018).
30. Schilling, R.- J., Carroll Jr., J.- J., Al-Ajlouni, A.-F.: Approximation of nonlinear systems with radial basis function neural networks. IEEE Trans. Neural Networks **12**(1) 1-15 (2001).
31. Sun, J., Zhou, A.: Finite Element Methods for Eigenvalue Problems, CRC Press Taylor & Francis Group (2016).
32. Xu, W., Xu, B., Guo, F.: Elastic properties of particle-reinforced composites containing nonspherical particles of high packing density and interphase: DEM-FEM simulation and micromechanical theory. Computer Methods in Applied Mechanics and Engineering **326** 122-143 (2017).
33. Yan, X.: Finite element modeling of consolidation of composite laminates. Acta Mechanica Sinica **22**(1) 62-67 (2006).
34. Zadler, B.- J.: Properties of Elastic Materials using Contacting and Non-Contacting Acoustic Spectroscopy. Ph.D. thesis, Colorado School of Mines, Golden, Colorado, USA (2005).
35. Zadler, B.- J., Scales, J.- A.: Monitoring crack-induced changes in elasticity with resonant spectroscopy. Journal of Applied Physics **104**(2) 023536 (2008).
36. Zhou, L., Ren, S., Liu, C., Ma, Z.: A valid inhomogeneous cell-based smoothed finite element model for the transient characteristics of functionally graded magneto-electro-elastic structures. Composite Structures **208** 298-313 (2019).
37. Zienkiewicz, O.- C.: Origins, Milestones and Directions of the Finite Element Method A Personal View, Handbook of Numerical Analysis: Techniques of Scientific Computing (Part 2), Vol. 5, P. G. Ciarlet and J. L. Lions, eds., North-Holland, Amsterdam (1997).
38. Zienkiewicz, O.- C.: The Finite Element Method, 5th ed., McGraw-Hill (2000).

ICCS Camera Ready Version 2021
To cite this paper please use the final published version:
DOI: 10.1007/978-3-030-77964-1_34